Chen *et al. Molecular Cancer* (2024) 23:248
https://doi.org/10.1186/s12943-024-02153-1

Molecular Cancer

RESEARCH Open Access

SARS-CoV-2 nucleocapsid protein interaction with YBX1 displays oncolytic properties through PKM mRNA destabilization

Xin Chen[1†], Baohong Jiang[2†], Yu Gu[1†], Zhaoyang Yue[1], Ying Liu[1], Zhiwei Lei[1,3], Ge Yang[4,5], Minhua Deng[6], Xuelong Zhang[1], Zhen Luo[1], Yongkui Li[1], Qiwei Zhang[1], Xuepei Zhang[7], Jianguo Wu[1^], Chunyu Huang[6,8*], Pan Pan[9,10*], Fangjian Zhou[6*] and Ning Wang[6,7*]

Abstract

Background SARS-CoV-2, a highly contagious coronavirus, is responsible for the global pandemic of COVID-19 in 2019. Currently, it remains uncertain whether SARS-CoV-2 possesses oncogenic or oncolytic potential in influencing tumor progression. Therefore, it is important to evaluate the clinical and functional role of SARS-CoV-2 on tumor progression.

Methods Here, we integrated bioinformatic analysis of COVID-19 RNA-seq data from the GEO database and performed functional studies to explore the regulatory role of SARS-CoV-2 in solid tumor progression, including lung, colon, kidney and liver cancer.

Results Our results demonstrate that infection with SARS-CoV-2 is associated with a decreased expression of genes associated with cancer proliferation and metastasis in lung tissues from patients diagnosed with COVID-19. Several cancer proliferation or metastasis related genes were frequently downregulated in SARS-CoV-2 infected intestinal organoids and human colon carcinoma cells. In vivo and in vitro studies revealed that SARS-CoV-2 nucleocapsid (N) protein inhibits colon and kidney tumor growth and metastasis through the N-terminal (NTD) and the C-terminal domain (CTD). The molecular mechanism indicates that the N protein of SARS-CoV-2 interacts with YBX1, resulting in the recruitment of *PKM* mRNA into stress granules mediated by G3BP1. This process ultimately destabilizes PKM expression and suppresses glycolysis.

Conclusion Our study reveals a new function of SARS-CoV-2 nucleocapsid protein on tumor progression.

†Xin Chen, Baohong Jiang and Yu Gu contributed equally to this work.

*Correspondence:
Chunyu Huang
huangchy@sysucc.org.cn
Pan Pan
panpan@jnu.edu.cn
Fangjian Zhou
zhoufj@sysucc.org.cn
Ning Wang
wangning07011992@163.com

Full list of author information is available at the end of the article

Keywords SARS-CoV-2, Cancer, Nucleocapsid protein, Stress granule, Glycolysis

Introduction

Severe acute respiratory syndrome coronavirus 2 (SARS-CoV-2) is a highly transmissible coronavirus responsible for the pandemic of 2019 (COVID-19) [1, 2]. SARS-CoV-2 is an enveloped, single-stranded, positive-sense RNA virus with a non-segmented genome ~ 30 kb in size [3]. As a member of the genus Betacoronavirus family, SARS-CoV-2 shares 79% genomic similarity with SARS-CoV and 50% with MERS-CoV [4]. The viral genome encodes 16 non-structural proteins (Nsps), which are essential for virus replication and pathogenesis; four structural proteins, including envelope (E), membrane (M), spike (S), and nucleocapsid (N); and nine other accessory factors [5, 6]. SARS-CoV-2 predominantly targets human pulmonary alveolar cells and gains access to the bloodstream in the lungs [7, 8]. Consequently, SARS-CoV-2 infections spread from the lungs to tissues expressing SARS-CoV-2 receptors, such as the gastrointestinal tract and kidney [9, 10].

Studies have demonstrated viruses account for approximately 15–20% of human cancer cases [11]. The exact carcinogenic mechanism of oncogenic viruses remains incompletely understood, potentially involving disruptions to host cell genetic stability, irregular cellular responses, and the latency/reactivation of the virus [12]. Conversely, certain viruses have demonstrated an ability to exhibit oncolytic properties, leading to the destruction of cancer cells. Specific viruses have shown the ability to possess oncolytic properties, resulting in the eradication of cancer cells [13]. On one hand, acute viral replication within cells can induce lytic cell death [14]. On the other hand, viruses might stimulate antiviral immune responses, thereby modulating the tumor immune microenvironment. Acute viral replication within cells can lead to lytic cell death, while viruses may also trigger antiviral immune responses, influencing the tumor immune microenvironment [15]. Additionally, oncolytic viruses have been associated with the suppression of tumor angiogenesis [16]. Consequently, utilizing oncolytic viruses offers a promising new avenue for tumor therapy.

Several population-based studies have highlighted that SARS-Cov-2 infection increases the risk of mortality and causes more severe symptoms in patients with cancer compared to the general population [17]. In particular, patients with stage IV metastatic cancer have a relatively high death rate and severe clinical symptoms, suggesting that SARS-Cov-2 may promote tumor progression [13]. Research indicates that cancer patients with various types of tumors vary in their susceptibility to SARS-CoV-2 infection and the outcomes of COVID-19 [18]. Patients with hematological malignancies, and lung cancer have the highest death rate of COVID-19-related death [17–20] whereas solid organ tumors showed no significant excess mortality risk after receiving chemotherapy [18]. Several case reports revealed an oncolytic role of SARS-CoV-2 in cancer patients. Some patients with hematological malignancies who recovered from SARS-CoV-2 infection have achieved remission without the need for any form of chemotherapy, radiotherapy, or surgical interventions [21–23]. SARS-CoV-2 infection may protect against blood cancer, such as acute myeloid leukemia, NK/T cell lymphoma, and Hodgkin lymphoma, by inducing an anti-tumor immune response [22–26]. In addition, three patients with metastatic colon cancer (CRC), displayed radiologic reduction of disease burden after recovery from COVID-19 [27]. The tumor derived from a clear cell renal cell carcinoma (ccRCC) patient showed 80% necrotic after recovery from COVID-19 [28]. Despite these observations, current studies remain insufficient to clarify the impact of SARS-CoV-2 on tumor progression.

In this study, we investigated the regulatory role of SARS-CoV-2 infection in solid tumor progression, including lung, colon, kidney and liver cancers. Our research revealed an association between SARS-CoV-2 infection and reduced cell proliferation, as well as decreased expression of genes related to cancer metastasis, in SARS-CoV-2 infected lung tissues, intestinal organoids and human colon carcinoma cells. Furthermore, we provide experimental evidence that the N-terminal (NTD) and the C-terminal domain (CTD) of SARS-CoV-2 N protein inhibit colon and kidney tumor cell growth and metastasis. Mechanistically, our research unveiled that through its interaction with YBX1, a multifunctional RNA-binding protein involved in mRNA co-transcriptional and translational regulation, the N protein recruits *PKM* mRNA into G3BP1-mediated stress granules (SG), resulting in the destabilization of PKM expression and the suppression of glycolysis resulting in cell apoptosis.

Methods

Ethic statement

The study follows the guidelines of the Care and Use of Laboratory Animals published by the US National Institutes of Health (NIH Publication No. 85−23, revised in 1996). All animal experiments were approved by the Institutional Animal Care and Use Committee (IACUC) of Jinan University and Sun Yat-sen University Cancer Center. Balb/c nude mice used in this study were ordered

from the Charles River Company (Beijing, China) and housed under specific-pathogen-free conditions.

Cell culture

HCT116, 786O, HEPG2, A549 and FHC cells were purchased from ATCC. All cell lines were maintained in an incubator at 37℃ with 5% CO2. HEPG2, 786O, A549, FHC, and HCOEPIC cells were cultured in Dulbecco's modified Eagle's medium (DMEM) (GIBCO, USA) supplemented with 10% Fetal Bovine Serum (FBS), 100 U/ml penicillin, and 100 mg/ml streptomycin sulfate. HCT116 cells were maintained in RPMI 1640 medium (GIBCO, USA) supplemented with 10% FBS, 100 U/ml penicillin, and 100 mg/ml streptomycin sulfate. All cultured cells were regularly tested and found to be mycoplasma free.

Gene set enrichment analysis (GSEA)

GSEA was applied to evaluate enriched cellular pathways and relevant molecular mechanisms. The GSEA software (version 3.0) was downloaded from GSEA website. A subset of c2.cp.kegg.v7.4.symbols.gmt was downloaded from the Molecular Signatures Database.

Colony-formation assay

Five hundred cells were seeded into each well of 6-well plates. Following a cultivation period of 10–14 days, the colonies were immobilized, subjected to staining, and subsequently enumerated.

Transwell assays

For the transwell experiments, 500 μl of cell culture medium with fetal bovine serum (FBS) was introduced into the lower compartment of the chamber (BD Biosciences, USA). 5×10^4 -2×10^5 cells suspended in 500 μl serum-free medium were subsequently plated into the upper insert of a 24-well plate. Following an incubation period of 24–36 h, the cells that had invaded were immobilized, subjected to staining, and subsequently enumerated under a microscope. All images were processed using ImageJ software.

Animal experiment

In various experimental models, animals were chosen at random, ensuring a minimum of five animals within each condition. All BALB/c nude mice (female, 18–20 g, four weeks old), utilized in the lung metastasis model, the bone metastasis model, and the subcutaneous xenograft model, were procured from Charles river Laboratory (Beijing, China).

In the subcutaneous xenograft model, a total of 5×10^6 HCT116 cells, HEPG2 cells or 786O cells were introduced into the right flank of each four-week-old BALB/c nude mouse. Tumor formation was assessed after 4–6 weeks.

For the lung metastasis model, 1×10^6 luciferase-transduced HCT116 cells or 4×10^6 A549 cells were injected into the tail vein of each four-week-old BALB/c nude mouse. Four to six weeks post-injection, the mice were sacrificed. The lungs were obtained and after fixation, embedding, and H&E staining, the number of metastatic lesions were calculated to evaluate tumor growth. To visualize the metastatic tumors, the IVIS 200 imaging system was employed after anesthetizing the mice with isoflurane and administering 100 μl of intraperitoneal VivoGlo™ luciferin solution (Promega, USA).

For bone metastasis model, 5×10^6 luciferase-transfected A549 cells transfected with N-Flag or control plasmids were injected into the left cardiac ventricle after anesthetized. 8 weeks later, the metastatic condition of bone was measured by IVIS 200 imaging system. Then the mice were euthanized and the marked bones were acquired and conducted H&E staining.

To determine the in vivo effect of N protein on tumor metastasis, 5×10^5 luciferase-transduced HCT116 cells were injected into the tail vein of 10 four-week-old BALB/c nude mice which were randomly divided into two groups. After 7 days when the inoculated tumor cells formed colonies in the lung, we directly intravenously injected purified SARS-CoV-2 N protein or PBS in the tail vein of BALB/c nude mice. Animals were given single injections with 10 mg/kg twice a day. After one month, the metastatic tumors were measured by IVIS 200 imaging system and then euthanized.

RNA immunoprecipitation (RIP)

The RNA Immunoprecipitation (RIP) procedure was executed following the guidelines of the Magna RIP RNA-Binding Protein Immunoprecipitation Kit (Millipore, USA). Cells were gathered and subjected to lysis buffer for a duration of thirty minutes at 4 °C. After centrifugation, the resulting lysates were collected and allowed to incubate overnight with 30 μl of Protein-A/G beads (Thermo Fisher Scientific, USA) with the appropriate antibodies. The beads were washed for 6 times. Before the immunoprecipitated RNA was extracted using TRIzol reagent (Invitrogen, USA) for subsequent sequencing analysis. The primary antibodies used for the RIP process in our investigation were as follows: anti-Flag-HRP (1:200, Cell Signaling Technology, USA, catalog number: 2368); anti-YBX1 (1:100, Abcam, catalog number: ab76149).

Preparation of RNA libraries and high-throughput sequencing

The quality and quantity of RNA was assessed by Agilent 2200 TapeStation (Agilent Technologies, USA) and Qubit (Thermo Fisher Scientific, USA). Briefly, RIP RNAs were fragmented to approximately 200 bp. Then, the RNA fragments were subjected to cDNA synthesis and

adaptor ligation following the instructions of NEBNext® Ultra RNA LibraryPrep Kit for Illumina (NEB, USA). The final library product was assessed with Agilent 2200 TapeStation and Qubit® (Life Technologies, USA) and then sequenced on Illumina (Illumina, USA) platform with pair-end 150 bp at Ribobio Co. Ltd (Ribobio, China). Date preprocessing Adaptor and low-quality bases were trimmed with Trimmomatictools (version:0.36), and the clean reads undergone rRNA deleting to get effective reads. Genomic alignment (version from UCSC genome browser) was using Tophatb (version:2.0.13) to get unique mapping reads.

Peaks calling and motif identification in RIP-Seq

Piranha (version 1.2.1) was employed to perform peak calling. Then using Hommer (version:4.8) to annotate the Peaks. The nucleotides in Peaks region were used for detection of the consensus motif by STREME (version: 5.3.0) and MEME (version:5.3.0). Motif central enrichment was performed by CentriMo (version:5.3.0).

Functional enrichment analysis

Gene ontology (GO) and Kyoto Encyclopedia of Genes and Genomes (KEGG) pathway enrichment analysis were performed using KOBAS3.0/ the clusterProfiler package. The enriched results were restricted to GO biological process and KEGG pathway terms. The GO biological process and KEGG pathway terms with adjusted P-value < 0.05 were considered to be significant.

Coimmunoprecipitation and mass spectrometry

Protein extraction from plasmid-transfected cells was carried out, and 1/10 protein lysis solution of each sample was obtained as input. The rest protein lysis solution was incubated with Flag (1:200, Cell Signaling Technology, USA, catalog number: 2368) antibodies followed by a 30-minute rotation at 4 ℃. Subsequently, samples were subjected to incubation with Sepharose-conjugated protein G magnetic beads (Thermo Fisher Scientific, USA) for overnight at 4 °C. After 4 times washing, the beads were suspended in 1× SDS and boiled for 10 min. Western blotting was then conducted to verify the IP efficiency. Mass spectrometry procedures were conducted by Wininnovate Bio (Shenzhen, China). Tandem mass spectrometry data were obtained using data-dependent acquisition mass spectrum techniques via a ThermoFisher Q Exactive mass spectrometer (Thermo Fisher Scientific, USA).

Western blotting

After PBS wash, the harvest cells were lysed by RIPA buffer. After 12,000 rpm centrifuge for 15 min, the supernatants were collected. The supernatant protein lysates subsequently were dissolved in 1× SDS buffer and separated through SDS-PAGE. Upon transferring to a PVDF membrane (Millipore, USA), the membrane was subjected to an overnight incubation at 4 °C with primary antibodies, followed by an additional 1 h incubation at room temperature with secondary antibodies. After washing for 3 times, the signals presenting on the membranes were visualized using an enhanced chemiluminescence kit (Tanon, China). For Western blotting in our study, the primary antibodies used included: rabbit polyclonal anti-Flag-HRP (1:1000, Cell Signaling Technology, USA, catalog number: 2368), PKM1/2 (1:500, Cell Signaling Technology, USA, catalog number: 3106), LDHA (1:1000, Cell Signaling Technology, USA, catalog number: 3582), BCL-2 (1:1000, Cell Signaling Technology, USA, catalog number: 4223), BAX (1:2000, Cell Signaling Technology, USA, catalog number: 5023), Caspase 3 (1:1000, Cell Signaling Technology, USA, catalog number: 9962), Cleaved Caspase 3 (1:1000, Cell Signaling Technology, USA, catalog number: 9661), PARP (1:2000, Cell Signaling Technology, USA, catalog number: 9532), Cleaved PARP (1:2000, Cell Signaling Technology, USA, catalog number: 5625), GAPDH (1:2000, Cell Signaling Technology, USA, catalog number: 2118), ACTIN (1:2000, Cell Signaling Technology, USA, catalog number: 4970).

Protein-protein interaction network

The protein-protein interaction network was built and visualized by using STRING software. The green, red, blue, black, cyan, and purple edges represent the predicted gene neighborhood interactions, gene fusions, gene co-occurrence interactions, co-expression interactions, known interactions from curated databases, and known interactions experimentally determined, respectively. Besides, the different color of nodes represents the included GO terms. The red nodes represent the mRNA processing terms (GO:0006397), the blue nodes represent the mRNA binding terms (GO:0003729).

Quantitative real-time polymerase chain reaction

Total RNA from the samples was extracted using TRIzol reagent (Invitrogen, USA). Subsequently, 1 μg of the extracted RNA underwent reverse transcription to cDNA, following the protocol outlined in the PrimeScript RT reagent kit (TaKaRa, JP). For quantitative real-time polymerase chain reaction (qRT-PCR), SYBR Green SuperMix (Roche, USA) was employed in combination with the ABI Prism 7000 Sequence Detection System (Applied Biosystems). The qRT-PCR data were analyzed using the Relative Quantification (ΔΔCT) method. The primer sequences utilized are listed as bellow:

PKM forward 5'-AGTACCATGCGGAGACCATC-3'
PKM reverse 5'-GCGTTATCCAGCGTGATTTT-3'
GAPDH forward 5'-CAGCCTCAAGATCATCAGCA-3'

GAPDH reverse 5'-ATGATGTTCTGGAGAGCCCC-3'

Immunofluorescence

Cultured cells were washed three times with cold PBS, and fixed with 4% paraformaldehyde (PFA) for 15 min. After 10 min incubation with 0.5% Triton X-100, cells were blocked with 5% BSA for 1 h at room temperature. They were then subjected to an overnight incubation with the primary antibody at 4 °C. On the next day, the cells were exposed to the corresponding secondary antibody for 1 h at room temperature and subsequently stained with DAPI. The images were captured using a Leica confocal microscopy system. The antibodies used in immunofluorescence were as follows: anti-Flag (Cell Signaling Technology, USA, catalog number: 2368) at a dilution of 1:100, and anti-G3BP1 (Abcam, UK, catalog number: ab181150) at a dilution of 1:200.

mRNA stability

10 μg/ml actinomycin D (ActD) was directly added into cells for the indicated times. The cells were harvested at indicated time after addition of ActD. mRNA amounts were measured by qRT-PCR as described above and normalized to Actin before calculation of half-lives.

Apoptosis analysis

Cultured cells were washed three times with cold PBS. Assessment of apoptosis was carried out using an Annexin V Apoptosis Detection Kit (Thermo Fisher Scientific, USA), following the manufacturer's instructions. In brief, the cells were suspended in 100 μL of binding buffer containing 5 μL of FITC-conjugated Annexin V antibody, followed by a 15-minute incubation at room temperature. Subsequently, they were washed and resuspended in 200 μL of binding buffer, to which 5 μL of propidium iodide (PI) was added. Finally, the cells were subjected to analysis using the CytoFlex flow cytometry system (Beckman Coulter, USA) and the FlowJo software (Treestar).

Seahorse experiment

XF96 analyzer (Agilent, Santa Clara, CA, USA) was used to conducted XF glycolysis stress test and mitochondrial stress test according to the manufacturer's instructions. Briefly, cells were seeded in Seahorse XF plates at a density of 5×10^4 per well and cultured for 24 h. The low buffered XF assay medium (Agilent, JP), supplemented with 10 mM glucose and 2 mM glutamine was used in the next day. Cells were then cultured for 1 h at 37 °C in a no-CO2 incubator. Seahorse XF analysis, Oxygen Consumption Rate (OCR = pmole O2/min) and ExtraCellular Acidification Rate (ECAR = mpH/min) were conducted at 37 °C.

Plasmid construction and transfection

The N gene of SARS-CoV-2 (GenBank accession number MN908947.3) were synthesized by GenScript, Nanjing, China, and cloned to pcDNA3.1(+) or plv lentivirus-expression vector with Flag-tag. The truncated DNA fragment of N mutant were amplified from pcDNA3.1(+)-N-Flag plasmid and inserted into pcDNA3.1(+) or plv lentivirus-expression vector with Flag-tag. Plasmid transfection was conducted using Lipofectamine 2000 (Invitrogen, CA, USA) or JetPEI (Polyplus).

Quantification and statistical analysis

All statistical analyses are described in the corresponding methods sections and indicated in the figure legends. Statistical analysis was carried out using GraphPad Prism 10. All results are presented as the mean ± SD or SEM. NS, no significance.

Results

Infection with SARS-CoV-2 is linked to reduced cell proliferation and downregulation of cancer metastasis-related pathways in lung, colon, and kidney tissues

To investigate the clinical relevance of SARS-CoV-2 infection in lung, colon, and kidney tissues, we conducted Gene Set Enrichment Analysis (GSEA) to assess the functional enrichment of significantly altered gene sets between control samples and those infected with SARS-CoV-2. GSEA analysis from the GEO database (GEO number: 150316) revealed that SARS-CoV-2 infection is negatively associated with cell migration and cancer metastasis in lung tissues derived from COVID-19-positive patients (Fig. 1A and B). Importantly, SARS-CoV-2 infection in lung tissues demonstrates a negative correlation with cancer survival outcomes (Fig. 1A). As SARS-CoV-2 can infect various organs, including the colon and kidney [29–34], our subsequent investigation focuses on understanding the pathological implications of SARS-CoV-2 infection in these organs. Our studies demonstrate that SARS-CoV-2 infection is negatively associated with cell proliferation and cancer metastasis in the colon (Fig. 1C and D) and kidney tissues (Fig. 1E and F) derived from COVID-19-positive patients. Furthermore, genes associated with cancer proliferation or metastasis exhibited significant downregulation in lung tissues obtained from patients with COVID-19 (Fig. 1G and H). Intestinal organoids are widely used to study gut infection by SARS-CoV-2 [35, 36]. GSEA analysis from human intestinal organoids (GEO number: GSE149312) revealed that SARS-CoV-2 infection is negatively associated with cancer metastasis in SARS-CoV-2 infected intestinal organoids (Fig. 2A). Heat map demonstrated that multiple cell proliferation, metastasis, and cell survival-related genes (Fig. 2B - D) were significantly downregulated in SARS-CoV-2 infected human intestinal organoids. These

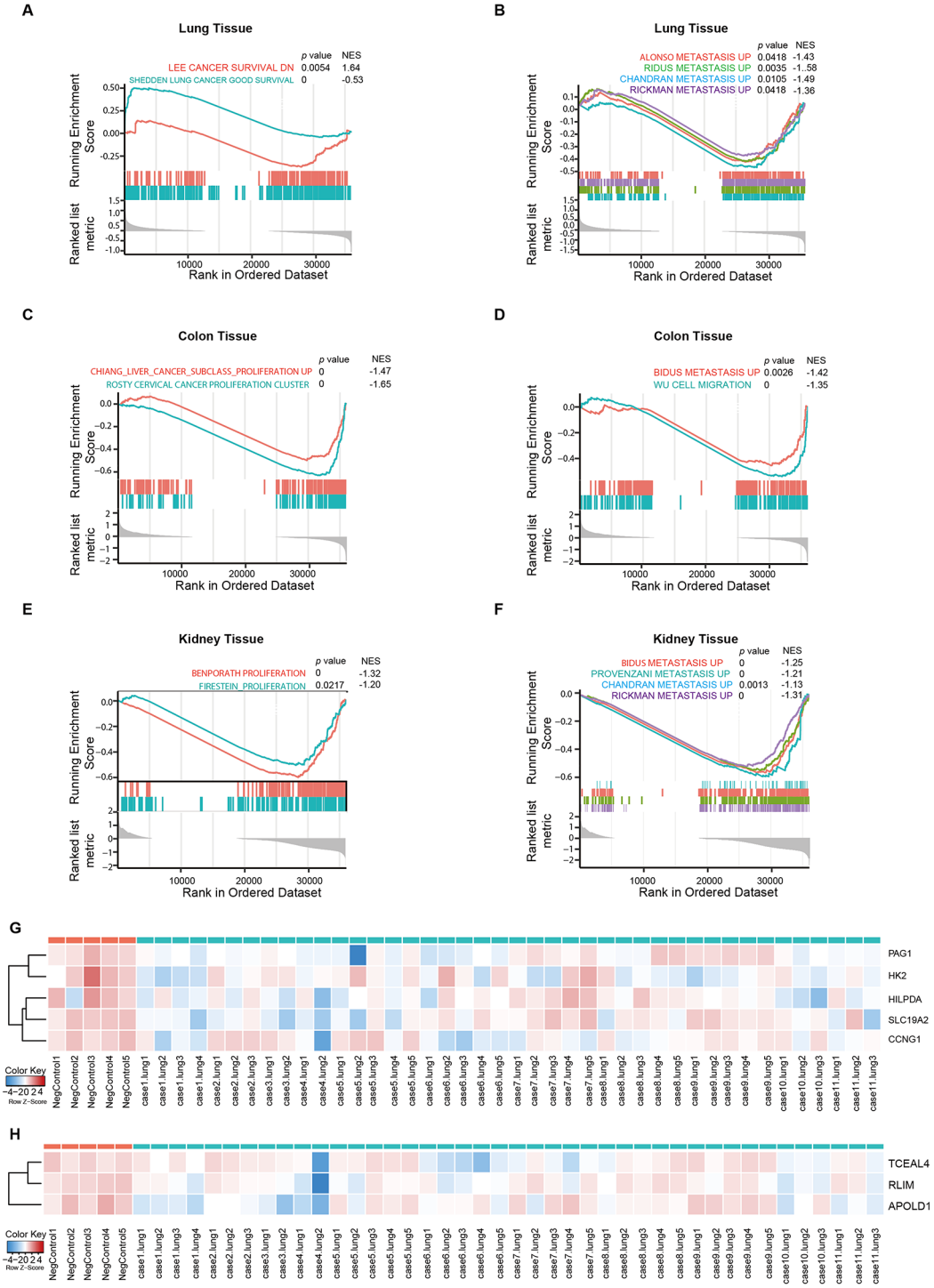

Fig. 1 SARS-CoV-2 infection shows a negative correlation with cell migration and cancer metastasis in lung, colon, and kidney tissues obtained from COVID-19-positive patients. **A–F** GSEA identified that SARS-CoV-2 infection is negatively associated with cancer proliferation, metastasis process, or poor survival in the lung (5 negative specimens *v.s.* 5 infected specimens), colon (5 negative specimens *v.s.* 4 infected specimens), and kidney (5 negative specimens *v.s.* 3 infected specimens) tissues derived from COVID-19-positive patients and negative controls. **G–H** The heat map showed downregulation of cancer proliferation and metastasis-related genes in the lung tissues derived from COVID-19-positive patients and negative controls

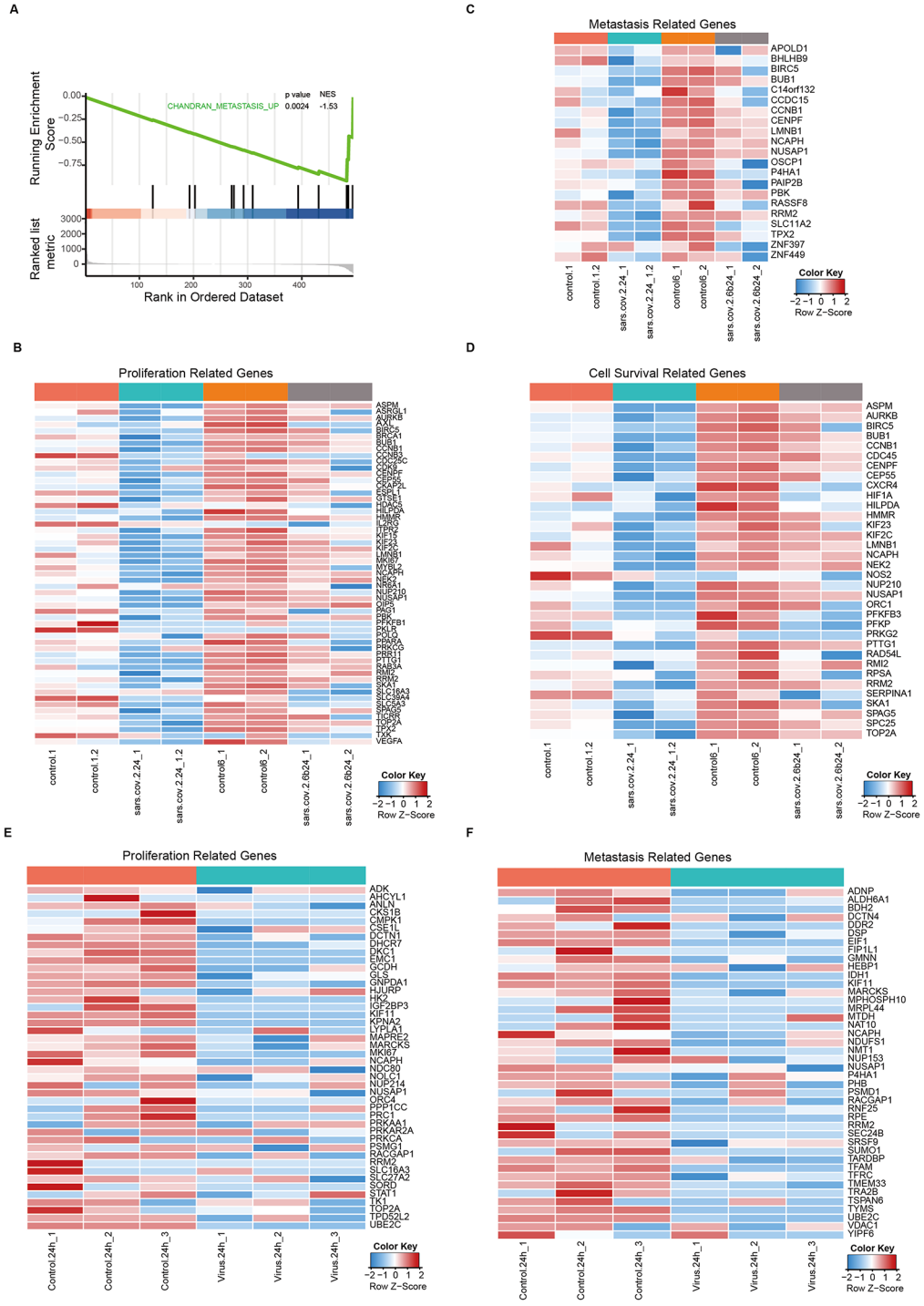

Fig. 2 SARS-CoV-2 infection is associated with downregulation of cell proliferation and cancer metastasis-related genes in SARS-CoV-2 infected human intestinal organoids and colon epithelial carcinoma cells. **A** GSEA analysis from human intestinal organoids revealed that SARS-CoV-2 infection is negatively associated with cancer metastasis in SARS-CoV-2 infected intestinal organoids. **B–D** Heat map demonstrated downregulation of cancer proliferation, metastasis, and cell survival-related genes in SARS-CoV-2 infected human intestinal organoids. **E-F** The heat map showed downregulation of cancer proliferation and metastasis-related genes from quantitative translatome data in the SARS-CoV-2 infected human colon epithelial carcinoma cells

findings indicate that SARS-CoV-2 infection might prevent the development and progression of cancer in the lungs, colon, and kidneys.

We next explore quantitative translatome data to investigate the role of SARS-CoV-2 infection in cancer cell growth and metastasis [37]. The heatmap of hierarchical clustering showed that several cancer proliferation and

metastasis-related proteins are frequently downregulated in SARS-CoV-2 infected human colon epithelial carcinoma cells, Caco-2 (Fig. 2E and F). These data suggest that SARS-CoV-2 may possess anti-tumor properties.

SARS-CoV-2 inhibits colon and kidney tumor cell growth through the N-terminal (NTD) and the C-terminal domain (CTD) of SARS-CoV-2 N protein

We then investigate the effects of the SARS-Cov-2 virus on tumor growth in human colon, kidney, and liver cancer cells, which represent target organs of SARS-Cov-2 infection [29–34]. In order to replicate the full SARS-CoV-2 infection process, we utilized replication-competent SARS-CoV-2-GFP/ΔN virus particles (trVLP), which lack the N gene, to co-infect cells along with SARS-CoV-2 N lentivirus (Fig. 3A) [38]. The replication-competent SARS-CoV-2-GFP/ΔN virus could efficiently infect HCT116, 786O, and HepG2 cells (Fig. S1A). We found that in SARS-CoV-2-GFP/ΔN virus and N lentivirus co-infected HCT116, 786O, and HepG2 cells, the colony formation was strongly inhibited (Fig. 3B). However, in uninfected control cells or SARS-CoV-2-GFP/ΔN virus alone infected cells, the colony formation was not affected (Fig. 3B), indicating that the N protein may have an inhibitory effect on tumor cell growth.

Consequently, we investigated the impact of the SARS-CoV-2 N protein on tumor growth in vitro. Our findings revealed that the expression of the SARS-CoV-2 N protein markedly suppressed colony formation (Fig. 3C and D) and cell growth (Fig. S1B) of HCT116, 786O, and HepG2 cells. In contrast, the SARS-CoV-2 N protein does not influence the growth of normal epithelial cells, such as FHC and HCOEPIC cells (Fig. S1C, D). Since the function of inhibiting proliferation was more significant in HCT116 and 786O cells (Fig. 3B and D), we next used these two cell lines to examine which domain of N protein contributed to tumor suppression. The N protein consists of five domains, including two RNA-binding domains: NTD, aa: 44–174 and CTD, aa:248–366; three intrinsically disordered regions (IDRs) (Nidr, aa:1–40; linker idr: aa:174–249; Cidr, aa: 365–419) (Nidr and linker idr involved in LLPS) [39]. We constructed a series of N variants by deleting one domain at a time (Fig. S1E) and found that compared with the cells transfected empty plasmid, the strong inhibition of colony formation occurred upon deletion of the three IDRs (N-Δ1, N-Δ3, N-Δ5). However, the deletion of NTD (N-Δ2) and CTD (N-Δ4) restored the colony formation ability (Fig. 3E). These results suggest that the N-terminal and the C-terminal domain of the SARS-CoV-2 N protein are both essential for tumor suppression in HCT116 and 786O cells. In vivo study further confirmed that constitutively expression of the N protein in HCT116, HEPG2 and 786O cells efficiently reduces the size and the weight of subcutaneous xenograft tumors (Fig. 3F - H).

SARS-CoV-2 N protein inhibits colon and kidney tumor metastasis in lung metastasis mouse model

We next evaluated the role of SARS-CoV-2 N protein on tumor metastasis. We used HCT116, 786O, HepG2, and A549 cells as representatives of SARS-Cov-2 infected organs, including colon, kidney, liver and lung [29–34]. In vitro assay demonstrated that the N protein inhibits colon, kidney, liver, and lung tumor cells' invasive capabilities (Fig. 4A). The deletion of three IDRs (N-Δ1, N-Δ3, N-Δ5) impaired cell migration ability of HCT116 and 786O cells when compared to the cells transfected empty plasmid. Importantly, the deletion of NTD (N-Δ2) and CTD (N-Δ4) restored cell migration ability (Fig. 4B). These results suggest that the NTD and the CTD of the SARS-CoV-2 N protein are both essential for tumor suppression in HCT116 and 786O cells.

Since lung and colon were important organs infected and injured by SARS-CoV-2 [40, 41], we used HCT116 and A549 cells to demonstrate the physiological significance of these results by a tail-vein injection lung metastasis model. Our data showed that nude mice injected with HCT116 (Fig. 4C and D) or A549 cells expressing the N protein (Fig. 4E and F) had fewer and smaller metastatic nodules in the lung when compared to control mice. Furthermore, in vivo bone metastasis mice model revealed that nude mice injected with N protein-expressed A549 cells had significantly fewer bone metastatic nodules when compared to control mice (Fig. 4G and H), although the tumor incidence was 2/5 in both the control and the N-Flag groups. To further determine the in vivo effect of N protein on tumor metastasis, luciferase-transduced HCT116 cells were injected into the tail vein of nude mice. We then administered purified SARS-CoV-2 N protein intravenously into the tail vein while the control groups received PBS. After 30 days post-injection, we noted a significant decrease in the formation of metastatic tumor nodules in the lungs of mice injected with the N protein (Fig. 4I and J). Collectively, these findings suggest that the SARS-CoV-2 N protein hinders the metastatic potential of tumor cells.

SARS-CoV-2 N protein interacts with YBX1 through CTD domain

To further explore the anti-tumor mechanism of SARS-CoV-2 N in HCT116 and 786O cells, we investigated cellular proteins that may interact with SARS-CoV-2 N in both cell types. Through Mass Spectrometry (MS) analyses, we detected 156 N-interacting cellular proteins in HCT116 cells and 61 in 786O cells. Additionally, we identified 24 cellular proteins that were common N-interacting proteins in both cell lines (Fig. 5A, Supplementary

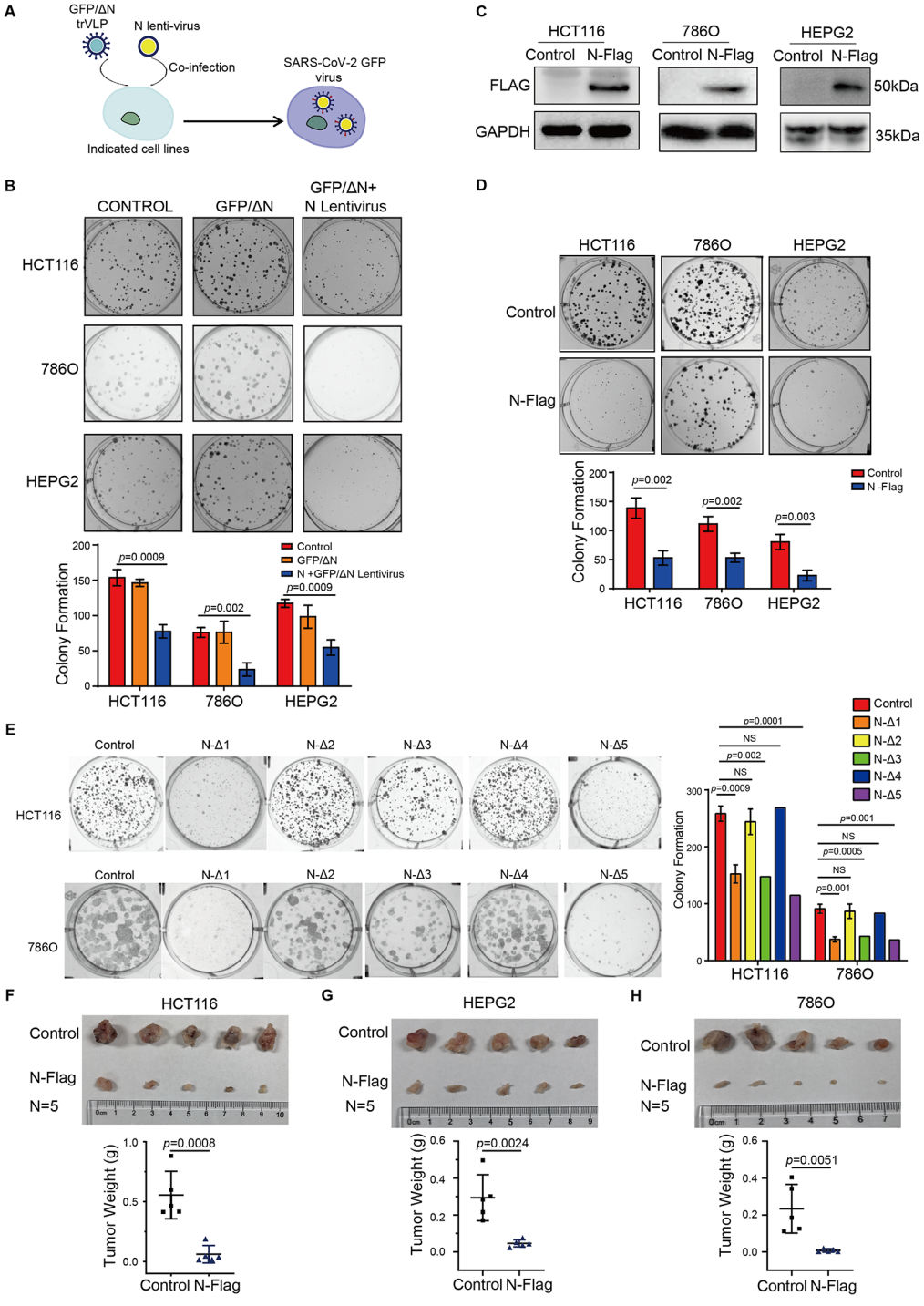

Fig. 3 The SARS-CoV-2 N protein inhibits colon and kidney tumor cell growth through the N-terminal (NTD) and the C-terminal domain (CTD). **A** A diagram illustrating the infection of replication-competent SARS-CoV-2-GFP/ΔN and N lenti-virus in colon, kidney, and liver tumor cells. **B** Colony formation in control, SARS-CoV-2-GFPΔN alone or GFPΔN virus and N lentivirus co-infected colon, kidney, and liver tumor cells. Paired *t-test* was used. **C** Immunoblot showed the expression of SARS-CoV-2 N protein expression in indicated cell lines. **D** Colony formation in control or SARS-CoV-2 N protein-expressed tumor cells. Paired *t-test* was used. **E** Colony formation in empty control or a series of N variants expressed in tumor cells. Paired *t-test* was used. **F–H** Subcutaneous xenograft tumor formation was performed on nude mice with control or SARS-CoV-2 N protein-expressed HCT116, HEPG2 and 786O cells. An unpaired *t-test* was used

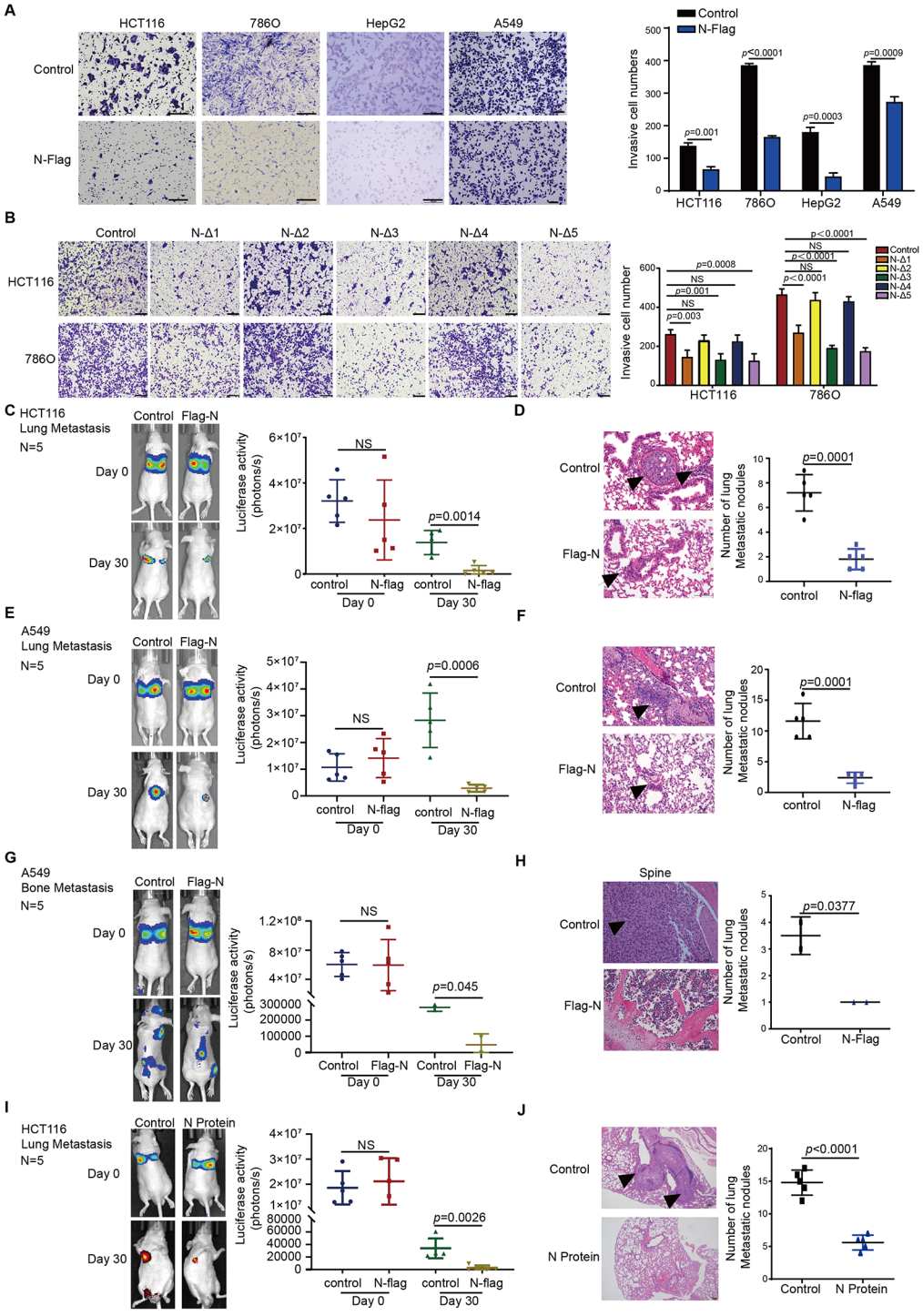

Fig. 4 SARS-CoV-2 N protein inhibits colon and kidney tumor metastasis in vivo. **A** Transwell assay showed the migration ability of control or SARS-CoV-2 N protein-expressed tumor cells. Paired *t*-test was used. **B** Transwell assay showed the migration ability of empty control or a series of N variants expressed in tumor cells. Paired *t*-test was used. **C–F** Tail-vein injection lung metastasis model showed tumor metastasis capacity in nude mice with control or SARS-CoV-2 N protein expressed HCT116 (**C-D**) and A549 cells (**E-F**). An unpaired *t*-test was used. **G-H***In vivo* bone metastasis mice model showed bone metastasis capacity in nude mice with control (2/5) or SARS-CoV-2 N protein (2/5) expressed A549 cells. An unpaired *t*-test was used. **I-J** Tail-vein injection lung metastasis model showed tumor metastasis capacity in mice injected with control or purified SARS-CoV-2 N protein. An unpaired *t*-test was used

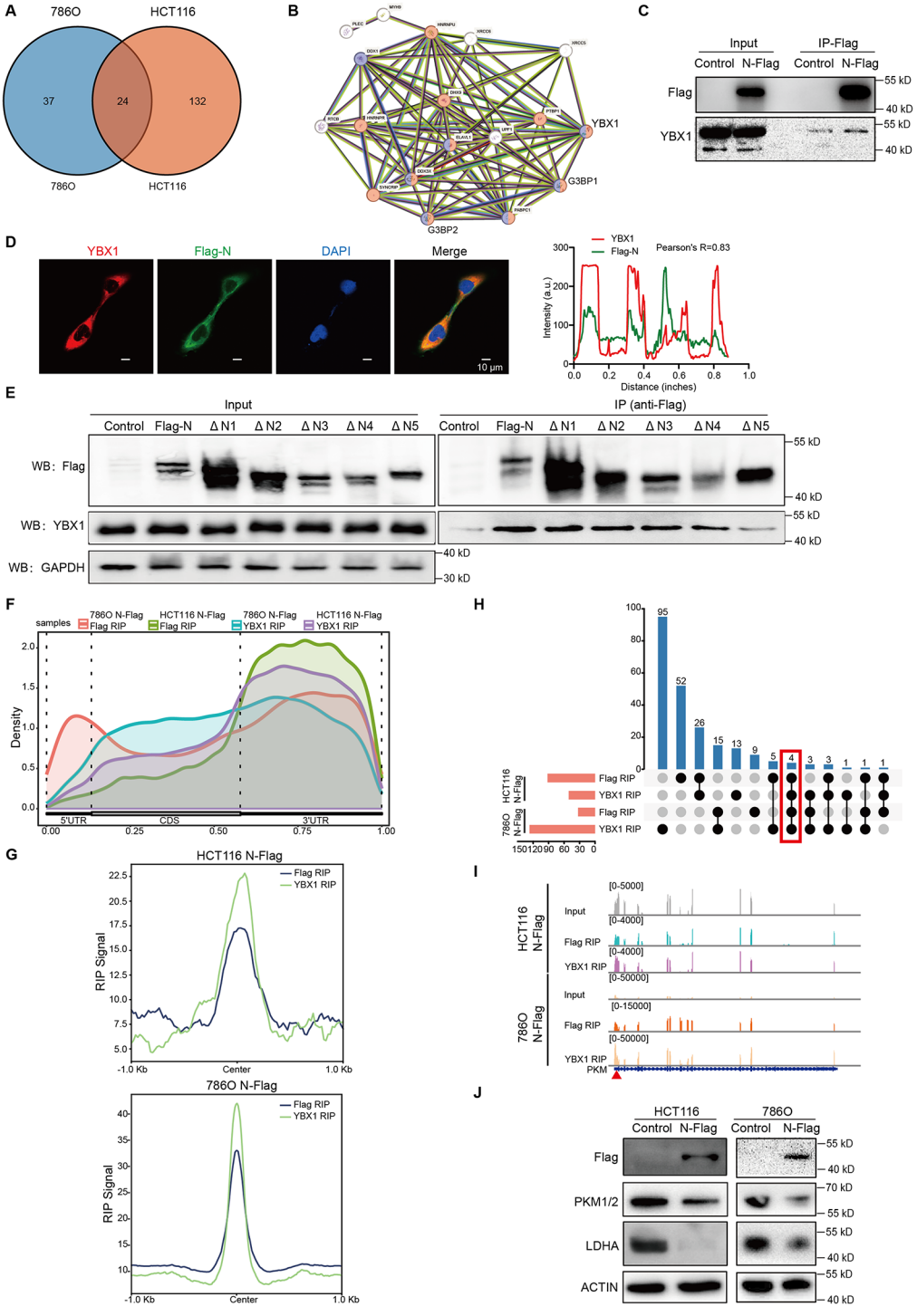

Fig. 5 SARS-CoV-2 N protein and YBX1 colocalized at 3′UTR of *PKM* mRNA and suppress PKM protein expression. **A** Mass spectrometry analysis showed that 24 common N-interacting proteins were identified in HCT116 and 786O cells. **B** Protein-protein interaction network analysis showed protein properties and connections of 24 common N-interacting proteins. The red nodes represent the mRNA processing terms (GO:0006397), the blue nodes represtent the mRNA binding terms (GO:0003729). **C-D** Immunoprecipitation (**C**) and confocal experiments (**D**) revealed the interaction and colocalization of N protein and YBX1 in HCT116 cells. **E** Immunoprecipitation experiments showed the interaction of N variants with YBX1 in HCT116 cells. **F** Metagene analysis by Guitar package indicated the peak distribution of 3′UTR, 5′UTR, and CDS regions of mRNAs binding to N protein or YBX1 in HCT116 and 786O cells. **G** Metagene analysis by deeptools showed the peak distribution of mRNAs binging to N protein and YBX1 in HCT116 cells (Upper) and 786O cells (Bottom). **H** The intersection of transcripts binding to N or YBX1 in HCT116 and 786O cells. **I** IGV diagram demonstrated the binding location of YBX1 and N protein on *PKM* in HCT116 and 786O cells. Genome hg38 was used as the reference. **J** Immunoblot showed the expression of glycolysis regulators in control or SARS-CoV-2 N protein-expressed cells

Table 1). Protein-protein interaction network analysis demonstrated that 6 common N-interacting proteins were involved in mRNA binding and stress granule (SG) cellular processes, including G3BP1, G3BP2, DDX3X, PABPC1, ELAVL1, and YBX1 (Fig. 5B). Immunoprecipitation (IP) and confocal experiments further confirmed that N protein colocalized and interacted with YBX1 in HCT116 cells (Fig. 5C and D). When compared to wild-type N protein, the interaction was notably reduced for the N protein mutated in the C-terminal domain (CTD) (Fig. 5E). These results suggest that the CTD of SARS-CoV-2 N protein plays essential roles in tumor suppression possibly through its interactions with N/YBX1.

SARS-CoV-2 N protein and YBX1 colocalized at 3'UTR of *PKM* mRNA and suppress PKM protein expression

As in the presence of C_{IDR}, NTD and CTD of N protein bind RNA to form a dimer or a higher-order structure to promote RNP packaging [42], we next performed RNA Immunoprecipitation sequencing (RIP-SEQ) in control or Flag-N overexpressing HCT116 and 786O cells to identify potential mRNAs bound to SARS-CoV-2 N protein. We purified Flag-tagged N protein-bounded cellular mRNA in both cells. Through peak calling comparison with HCT116 control cells, 4281 peaks were identified, covering 2328 N bound mRNAs; whereas in 786O cells, 14,365 peaks were identified, covering 4315 N bound mRNAs (Fig. 5F). Peak distribution analysis indicated that 58% and 38% of N peaks were located in regions encompassing the annotated 3'UTRs of the target RNA transcripts in HCT116 and 786O cells, respectively (Fig. S2A). Motif analysis further identified A/U-rich sequences as the most significantly enriched motifs in N-binding sites (Fig. S2B). Peak calling identified 1209 common host genes recruited to the Flag-N protein in HCT116 and 786O cells (Fig. 5F). KEGG analysis showed that N-bound genes were significantly enriched for several cancer-related pathways, including p53, cell-cycle, and apoptosis pathway ($P<0.05$) (Fig. S2C). Among these mRNAs, some were involved in cellular developmental processes (e.g., *MTCH1*, *CPNE1*, and *CAPN2*), regulation of cell death (*RPL10*, *IRS2*, and *CCAR2*), and apoptotic processes (*TFRC*, *PARK7*, and *PHB2*). Our data suggested that the N protein is likely to target growth-related genes in infected cells.

We next wonder whether the N protein could affect the expression of YBX1-bound cellular RNAs. We purified YBX1-bound RNAs from Flag-N overexpressing HCT116 and 786O cells. Through small RNA sequencing and peak calling comparison to input, 6403 peaks were identified, covering 3702 YBX1 bound mRNAs in HCT116 cells. In addition, 9547 peaks were identified, covering 3859 YBX1 bound mRNAs in 786O cells (Fig. 5F). Peak distribution demonstrated that 55% and 35% percentage of YBX1 peaks were found within the annotated 3'UTRs of the target transcripts in Flag-N expressing HCT116 and 786O cells, respectively (Fig. S2D). Similar to the results described above, motif analysis identified A/U-rich sequences as the most significantly enriched motifs in YBX1-binding sites in HCT116 cells (Fig. S2E). Peak calling identified 246 common host genes recruited at YBX1 in Flag-N expressing HCT116 and 786O cells (Fig. 5F). These YBX1 peaks in N-expressing cells were concentrated around the N-binding sites (Fig. 5G). KEGG analysis indicated that YBX1-bound genes were significantly enriched for pancreatic cancer, renal cell carcinoma, colon cancer-related pathways, and apoptosis pathways (Fig. S2F) ($P<0.05$). When comparing N-bound transcripts with those bound by YBX1, we noticed that four of the YBX1-bound transcripts overlapped with N-bound transcripts in N-expressing cells. These transcripts included *PKM*, *PABPC1*, *RN7SK*, and *RN7SL1* (Fig. 5H).

Among these genes, PKM, which is associated with glycolysis and cancer, was found to have a binding site for N in its 3'UTR, which overlapped with a binding site for YBX1 in N-expressing HCT116 and 786O cells (Fig. 5I). To test whether *PKM* is a target of the N protein, we examined the expression of *PKM* in N-expressed HCT116 and 786O cells. We found that PKM protein expression was strongly inhibited in N-expressed HCT116 and 786O cells (Fig. 5J). Moreover, LDHA expression, which is the downstream of PKM-glycolysis pathway, was also downregulated (Fig. 5J).

The interaction with YBX1 is essential for the recruitment of *PKM* mRNA into G3BP1-mediated stress granules by the SARS-CoV-2 N protein

Our MS analysis revealed that the N protein interacts with YBX1, G3BP1, and G3BP2, which are all involved in the stress granule (SG) pathway. The function of SGs during viral infection remains largely unknown. A recent study revealed that SGs are ribonucleoprotein (RNP) complexes containing both translationally stalled and translational compatible mRNAs [43] together with several RNA binding proteins (RBPs), including YBX1 [44, 45]. As SARS-CoV-2 N protein has been shown to interact with G3BP1 to suppress SG assembly [46–48], we speculated that N/YBX1 protein interactions could contribute to this process. SGs were visualized by immunostaining for G3BP1, an SG marker. The confocal experiment showed that under normal conditions, the N protein is colocalized with G3BP1 (Fig. 6A). Knockdown of YBX1 in HCT116 control cells did not interfere with the localization of G3BP1, while depletion of YBX1 in SARS-CoV-2 N expressed cells disrupted the colocalization of N and G3BP1 protein (Fig. 6A). Exposure to heat shock significantly induced the formation of G3BP-mediated SGs in control cells. However, in cells expressing the

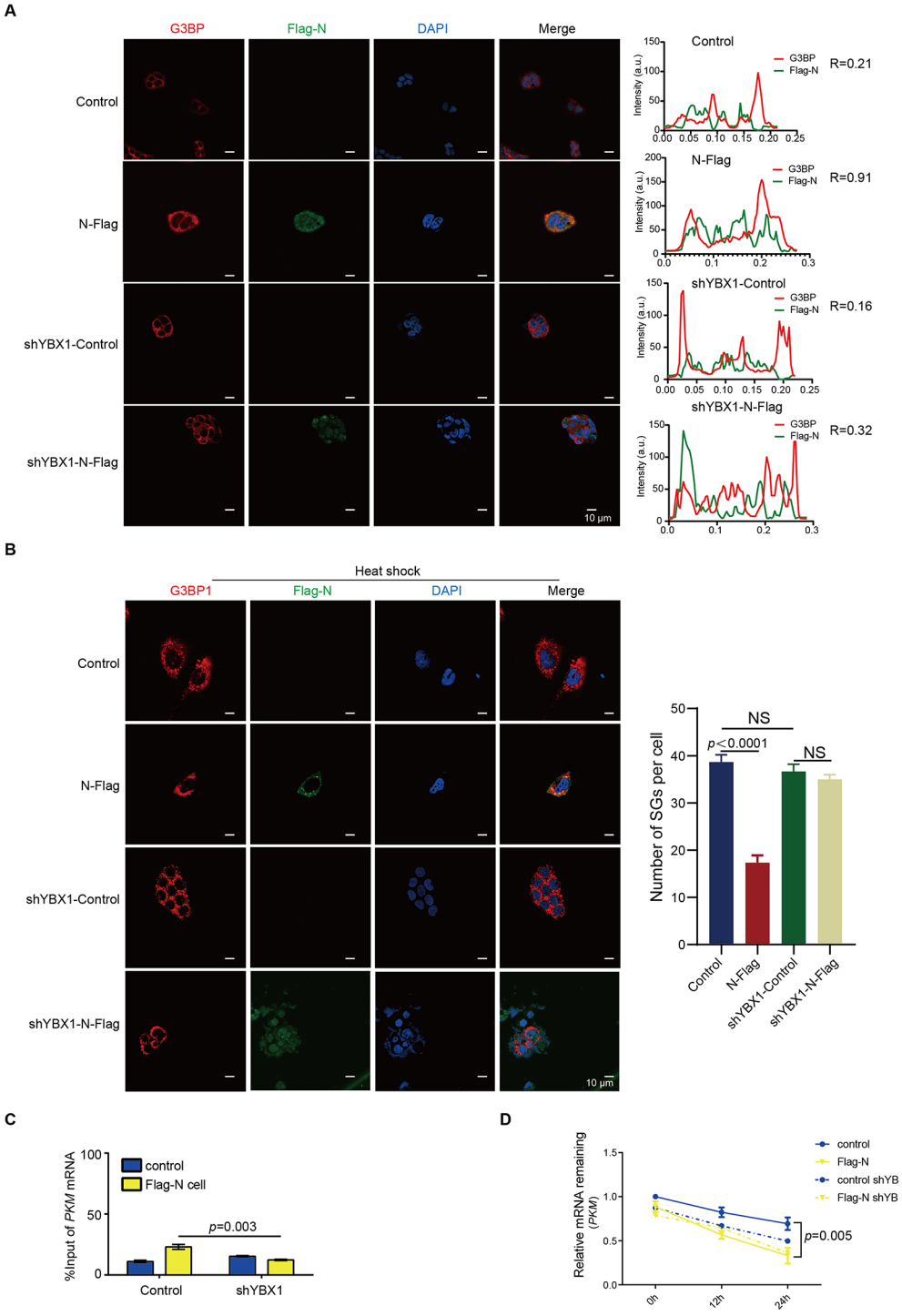

Fig. 6 The involvement of YBX1 is essential for the recruitment of PKM mRNA into G3BP1-mediated stress granules by the SARS-CoV-2 N protein. **A** Confocal experiments revealed the interaction and colocalization of N protein and G3BP1 in control or Flag-N expressed HCT116 cells with or without YBX1. **B** Confocal experiments revealed the interaction and colocalization of N protein and G3BP1 in heat shock treated in control or Flag-N expressed HCT116 cells with or without YBX1. Paired *t-test* was used. **C** RIP-qRT-PCR analysis revealed the enrichment of *PKM* mRNA in G3BP1-mediated stress granules isolated from control or Flag-N expressed HCT116 cells with or without YBX1. Paired *t-test* was used. **D** mRNA stability assay revealed the *PKM* mRNA stability in control or Flag-N expressed HCT116 cells with or without YBX1. Paired *t-test* was used

N protein, we observed colocalization of the N protein with G3BP1 in stress granules, while the formation of SGs was inhibited (Fig. 6B). Furthermore, reducing YBX1 levels in control cells did not disrupt the formation of G3BP-mediated SGs. However, when YBX1 was depleted in N-expressing cells, the colocalization of N and G3BP1 proteins decreased, and SGs formation was restored (Fig. 6B). These data indicated that the interaction with YBX1 is crucial for the localization of SARS-CoV-2 N protein within G3BP1-mediated stress granules.

We next investigated whether the N/YBX1 complex may recruit *PKM* mRNA into G3BP-mediated SGs and reduce *PKM* mRNA stability. We purified G3BP1-bound RNAs in control and N-expressed HCT116 cells [49]. RIP-PCR analysis revealed that in N-expressed cells, *PKM* mRNA was greatly enriched in the G3BP1 complex when compared to control cells (Fig. 6C). However, in cells expressing N where YBX1 was depleted, the recruitment of *PKM* mRNA with G3BP1 was significantly diminished (Fig. 6C). These data indicated that the interaction with YBX1 is indispensable for the SARS-CoV-2 N protein to recruit *PKM* mRNA into G3BP1-mediated SG.

SARS-CoV-2 N protein destabilizes the stability of *PKM* mRNA via its interaction with YBX1

Since SGs represents sites of mRNA triage for regulating mRNA stability and translatability [50], we hypothesized that the SARS-CoV-2 N protein may affect the stability of *PKM* mRNA by recruiting it into G3BP1-mediated SG. Following actinomycin D treatment, *PKM* mRNA stability was decreased in N-expressing HCT116 cells when compared to control cells. However, in N-expressed HCT116 cells depleted for YBX1, we did not observe an effect on *PKM* mRNA stability which contrasts to YBX1 knockdown control cells not expressing the N protein. These data demonstrate that the SARS-CoV-2 N protein impairs the stability of *PKM* mRNA stability via interaction with YBX1 (Fig. 6D).

Infection with SARS-CoV-2 suppressed glycolysis via the N/PKM/LDHA regulatory pathway

We conducted GSEA to identify cellular mRNA bound to Flag-RIP Seq and YBX1-RIP Seq and the cellular processes affected. Results from these studies indicated that bound RNA transcripts were enriched in the glycolysis pathway in both N or YBX1 RIP-Seq from HCT116 and 786O cells when compared to control cells. (Figure 7A and B). These analyses collectively suggest that the N protein might influence the cellular glycolysis process. Extracellular acidification rate (ECAR) analysis revealed that expression of N protein caused a dramatic reduction of glycolytic function, glycolysis, and glycolytic capacity in HCT116 cells (Fig. 7C and D). Furthermore, GSEA analysis conducted on mock or SARS-CoV-2 infected human intestinal organoids revealed an inverse correlation between SARS-CoV-2 infection and the glycolysis pathway (Fig. 7E). Indeed, the heatmap of hierarchical clustering further demonstrated that gene transcripts contributing to glycolysis were reduced in SARS-CoV-2-infected human intestinal organoids (Fig. 7F). Finally, the quantitative translatome analysis showed that in SARS-CoV-2 infected human colon epithelial carcinoma cells, glycolysis-related genes, such as LDHA are significantly downregulated (Fig. 7G). Collectively, these data demonstrate that SARS-CoV-2 infection inhibited glycolysis in human cancer cells.

SARS-CoV-2 N protein induces mitochondrial-dependent apoptotic pathway

Recent studies revealed that PKM plays a crucial role in controlling mitochondrial apoptosis progression [51, 52]. Since elevated levels of mitochondrial ROS can initiate apoptosis, we first tested whether the N protein may be involved in the regulation of mitochondrial ROS. To this end, cells were stained with MitoSOX red and relative signal intensities were quantified using a confocal fluorescence microscope. The results revealed high levels of mitochondrial ROS production in N protein-expressed HCT116 cells when compared to control HCT116 cells (Fig. 7H). We next performed Annexin V-FITC/PI staining and flow cytometry analysis for assessment of apoptosis in colon cancer cells. As shown in Fig. 7I, the proportion of apoptotic cells were significantly increased following the SARS-CoV-2 N protein expression. Moreover, the N protein induced the expression of pro-apoptotic proteins, BAX, cleaved-caspase 3, and cleaved-PARP in colon cancer cells (Fig. 7J). On the contrary, the antiapoptotic protein BCL-2 was downregulated by the expression of the N protein (Fig. 7J). Collectively, these data demonstrate SARS-CoV-2 N protein could induce apoptosis in colon cancer cells via mitochondrial-derived ROS production.

Discussion

The outbreak of SARS-CoV-2 caused a global pandemic that has raised international health concerns about coronaviruses [53]. Preliminary studies suggest that cancer patients are generally more vulnerable to SARS-CoV-2 infections when compared to individuals without cancer [17]. However, the impact of SARS-CoV-2 infection on the outcome of patients with cancer is controversial. It has been suggested that cancer patients with different tumor types have differing susceptibility to SARS-Cov-2 infection and COVID-19 disease outcome [18]. In contrast to patients with hematological malignancies and lung cancer, who have the highest death rate of COVID-19-related death [17–20]; chemotherapy-treated solid organ tumors patients showed no significant excess

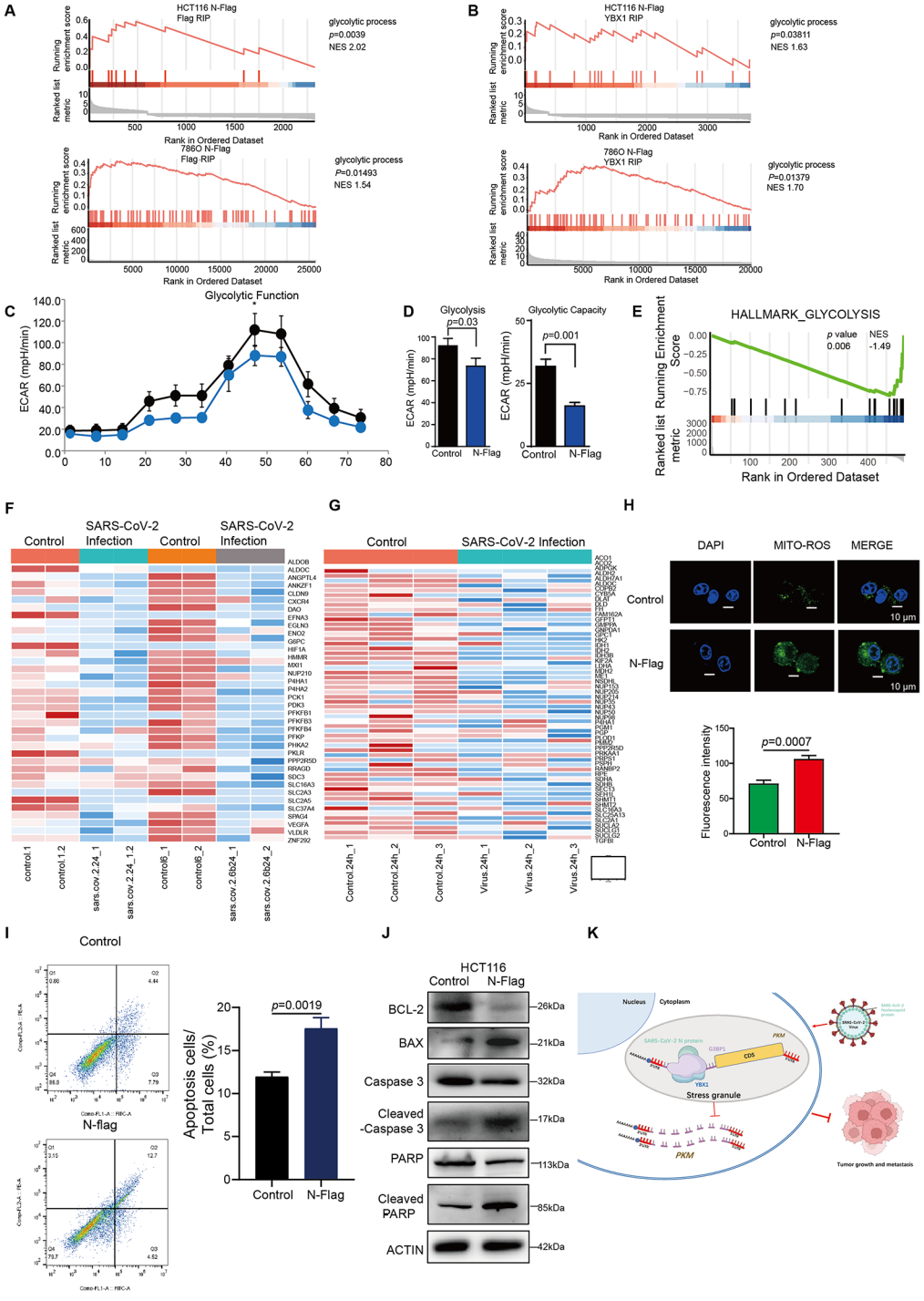

Fig. 7 SARS-CoV-2 infection inhibits glycolysis through SARS-CoV-2 N protein targeted PKM/LDHA pathway. **A-B** GSEA analysis from Flag-RIP Seq (A) and YBX1-RIP Seq (B) revealed that Flag-tagged N protein (A) and YBX1-bound RNAs (B) were enrichment in glycolysis in HCT116 and 786O cells. **C-D** ECAR analysis showed glycolytic function, glycolysis, and glycolytic capacity in control or SARS-CoV-2 N protein-expressed HCT116 cells. A paired *t-test* was used. **E** GSEA analysis from human intestinal organoids revealed that SARS-CoV-2 infection is negatively associated with glycolysis in SARS-CoV-2 infected intestinal organoids. **F-G** The heat map showed downregulation of glycolysis-related genes in SARS-CoV-2 infected human intestinal organoids (F) or from quantitative translatome data in SARS-CoV-2 infected human colon epithelial carcinoma cells (G). **H** Mitochondrial ROS produced in control or SARS-CoV-2 N protein expressed cells. A paired *t-test* was used. **I** Flow cytometry demonstrated cell apoptosis in control or SARS-CoV-2 N protein-expressed cells. A paired *t-test* was used. **J** Immunoblot showed apoptotic protein expression in control or SARS-CoV-2 N protein-expressed cells. **K** The working model showed SARS-CoV-2 N protein interaction with YBX1 in SG displays oncolytic properties through PKM mRNA destabilization.

mortality risk from COVID-19 [18]. Therefore, we aimed to evaluate the clinical and functional role of SARS-CoV-2 on solid tumor. Herein, we investigated the clinical significance of SARS-CoV-2 infection in lung, colon, and kidney organs. We found that SARS-CoV-2 infection was associated with decreased cancer metastasis and cell proliferation in colon and kidney tissues derived from COVID-19-positive patients.

This study provided the first experimental evidence that SARS-CoV-2 inhibit proliferation and induces cell death in several solid tumors, including colon cancer and kidney cancer. To this date, few studies have followed up on COVID-19 patients with cancer to monitor tumor progression. Case studies from a few groups reported that cancer patients with hematological cancer or CRC, experienced a tumor reduction or remission after SARS-CoV-2 infection [21–28]. It is important to clarify any definitive link between SARS-CoV-2 infection and tumor progression. Here, we demonstrate that SARS-CoV-2 inhibits colon, kidney, and liver tumor cell growth and metastasis *in vivo* and *in vitro* through the N-terminal (NTD) and the C-terminal domain (CTD) of SARS-CoV-2 N protein. We found that in SARS-CoV-2-GFP/ΔN virus and N lentivirus co-infected HCT116, 786O, and HepG2 cells, or N-overexpressed cells, cancer growth and metastasis were strongly inhibited.

Currently, although the molecular and cellular mechanism of oncolytic in antitumor actions remains poorly understood, it has been demonstrated that oncolytic virus could induce bust replication in a host cell which directly causes cell lytic death and reduces tumor volume [13, 14]. In addition, the oncolytic virus may destroy the tumor immune microenvironment, which subsequently triggers anticancer immune responses or inhibit tumor angionesis [14–16]. Upon stress or viral infections, host mRNAs, translation factors, and RBPs have been found sequestered into SGs [54]. Thus, SGs have been widely considered to play critical roles in the regulation of RNA storage, mRNA stabilization and translation, cell signaling, and apoptosis under stress [43]. Recently, SGs have gained increasing attention in cancer research by implicating various tumor-associated signaling pathways, including cell growth, metastasis, apoptosis, and so on [55]. Here, we identified that the SARS-CoV-2 N protein interacts with YBX1, a multifunctional RBP that is implicated in mRNA splicing, stabilization, translation, and RNA degradation [56, 57] and an important oncogene among various types of tumors [58]. Our studies revealed that by interacting with YBX1, the N protein recruits *PKM* mRNA into G3BP1-mediated SG, which consequently led to the destabilization of *PKM* expression and suppression of glycolysis (Fig. 7K).

Glycolysis is a vital metabolism promoting cancer growth, invasiveness and metastasis [59]. *PKM* is one of the key genes involved in glycolysis, encoding two isoenzymes: PKM1 and PKM2, catalyzing the step from phosphoenolpyruvate to pyruvate [60]. Subsequently, LDHA mediates the catalysis of pyruvate to lactate [61]. Our research uncovered that the N protein resulted in the downregulation of PKM2 and LDHA, leading to a significant decrease in glycolytic function, glycolysis, and glycolytic capacity in HCT116 cells. Moreover, GSEA analysis from SARS-CoV-2 infected human intestinal organoids identified that SARS-CoV-2 infection is correlated with lower *LDHA* expression, and inhibition of the glycolysis pathway. Besides the vital roles in promoting cell proliferation, the PKM gene is also implicated in cell apoptosis progression [51, 52]. PKM2 has been shown to inhibit apoptosis induced by ROS through the caspase-dependent pathway [51, 52]. The enhanced glycolysis by PKM2 can attenuate cell apoptosis in cancer cells. Consistently, we demonstrated that the SARS-CoV-2 N protein could induce apoptosis in colon cancer cells via mitochondrial-derived ROS production through *PKM* regulation. Our results suggest that the SARS-CoV-2 N protein could be used as an anti-cancer agent and warrant further studies.

It is promising to explore the oncolytic virotherapy of SARS-CoV-2 N protein. So far, several oncolytic viruses have been approved globally for the treatment of advanced cancers [62]. Oncolytic viruses could use the ability of replication competent to infect and kill tumor cells while not affecting non-tumor cells [63]. DNA viruses are more likely to be explored oncolytic function due to their molecular biology and life cycle are currently better understood [63]. Edward M Kennedy et al. develop Synthetic RNA viruses consisting of a viral RNA genome formulated within lipid nanoparticles [64]. In this study, we found that SARS-CoV-2 N protein could anti-tumor, while how to specifically target tumor cells and necessary preclinical studies were needed.

Supplementary Information

The online version contains supplementary material available at https://doi.org/10.1186/s12943-024-02153-1.

Supplementary Material 1

Supplementary Material 2

Acknowledgements

This work was supported by the National Natural Science Foundation of China (81730061 to J.W., 82072834 to X.C., 32200117 to P.P.) and the Guangdong Basic and Applied Basic Research Foundation (2021A1515011065 and 2023A1515010318 to X.C.)

Author contributions

XC, NW, PP, FJZ and JGW contributed to the conception of the project. XC, NW, PP, FJZ and JGW contributed to the design the project, and XC, NW, BHJ, YG, CYH contributed to the drafting of the manuscript. ZYY, YL, ZWL, GY, MHD and XLZ helped to perform the analysis. ZL, YKL, QWZ, and XPZ contributed to the reagents. All authors contributed to the article with constructive discussions and approved the submitted version.

Funding
National Natural Science Foundation of China, Grant/Award Number: 81730061, 82072834, 32200117; Guangdong Basic and Applied Basic Research Foundation, Grant/Award Number: 2021A1515011065,2023A1515010318; Natural Science Foundation of Hunan Province, Grant/Award Number: No. 2023JJ60495.

Data availability
The accession number of Mass Spectrometry data in iprox: IPX0007856000, IPX0007791000. The accession number of RIP-Seq data in SRA: SUB14102009.

Declarations

Ethics approval and consent to participate
The study follows the guidelines of the Care and Use of Laboratory Animals published by the US National Institutes of Health (NIH Publication No. 85 – 23, revised in 1996). All animal experiments were approved by the Institutional Animal Care and Use Committee (IACUC) of Jinan University and Sun Yat-sen University Cancer Center. Balb/c nude mice used in this study were ordered from the Charles River Company (Beijing, China) and housed under specific-pathogen-free conditions.

Consent for publication
Not applicable.

Competing interests
The authors declare no competing interests.

Author details
[1]Institute of Medical Microbiology, Key Laboratory of Viral Pathogenesis & Infection Prevention and Control, Jinan University, Ministry of Education, Guangzhou 510632, China
[2]Department of Pharmacy, The First Affiliated Hospital, Hengyang Medical School, University of South China, Hengyang 421001, China
[3]Qingyuan People's Hospital, The Sixth Affiliated Hospital of Guangzhou Medical University, Qingyuan 511500, China
[4]Foshan Institute of Medical Microbiology, Foshan 528315, China
[5]Section of Cellular and Molecular Biology, The Hormel Institute, University of Minnesota, Austin, MN 55912, USA
[6]State Key Laboratory of Oncology in South China, Guangdong Provincial Clinical Research Center for Cancer, Sun Yat-Sen University Cancer Center, Guangzhou 510060, China
[7]Department of Urology, The First Affiliated Hospital of Zhengzhou University, Zhengzhou 450003, China
[8]Department of Gastroenterology, The Third Affiliated Hospital of Guangzhou University of Chinese Medicine, Guangzhou 510000, China
[9]School of Basic Medical Science, State Key Laboratory of Respiratory Disease, Guangzhou Medical University, Guangzhou 511436, China
[10]The First Affiliated Hospital of Jinan University, Guangzhou 510632, China

Received: 10 March 2024 / Accepted: 10 October 2024
Published online: 06 November 2024

References

1. Ke Z, Oton J, Qu K, Cortese M, Zila V, McKeane L, Nakane T, Zivanov J, Neufeldt CJ, Cerikan B, et al. Structures and distributions of SARS-CoV-2 spike proteins on intact virions. Nature. 2020;588:498–502.
2. Tay MZ, Poh CM, Rénia L, MacAry PA, Ng LFP. The trinity of COVID-19: immunity, inflammation and intervention. Nat Rev Immunol. 2020;20:363–74.
3. Hu B, Guo H, Zhou P, Shi ZL. Characteristics of SARS-CoV-2 and COVID-19. Nat Rev Microbiol. 2021;19:141–54.
4. Munshi I, Khandvilkar A, Chavan SM, Sachdeva G, Mahale SD, Chaudhari UK. An overview of preclinical animal models for SARS-CoV-2 pathogenicity. Indian J Med Res. 2021;153:17–25.
5. Jackson CB, Farzan M, Chen B, Choe H. Mechanisms of SARS-CoV-2 entry into cells. Nat Rev Mol Cell Biol. 2022;23:3–20.
6. V'Kovski P, Kratzel A, Steiner S, Stalder H, Thiel V. Coronavirus biology and replication: implications for SARS-CoV-2. Nat Rev Microbiol. 2021;19:155–70.
7. Oroojalian F, Haghbin A, Baradaran B, Hemmat N, Shahbazi MA, Baghi HB, Mokhtarzadeh A, Hamblin MR. Novel insights into the treatment of SARS-CoV-2 infection: an overview of current clinical trials. Int J Biol Macromol. 2020;165:18–43.
8. Stein SR, Ramelli SC, Grazioli A, Chung JY, Singh M, Yinda CK, Winkler CW, Sun JF, Dicker JM, er al. SARS-CoV-2 infection and persistence in the human body and brain at autopsy. Nature. 2022;612:758–63.
9. Brogan M, Ross MJ. COVID-19 and kidney disease. Annu Rev Med. 2023;74:1–13.
10. Letko M, Marzi A, Munster V. Functional assessment of cell entry and receptor usage for SARS-CoV-2 and other lineage B betacoronaviruses. Nat Microbiol. 2020;5:562–9.
11. Krump NA, You J. Molecular mechanisms of viral oncogenesis in humans. Nat Rev Microbiol. 2018;16:684–98.
12. Song Y, Xu Y, Pan C, Yan L, Wang ZW, Zhu X. The emerging role of SPOP protein in tumorigenesis and cancer therapy. Mol Cancer. 2020;19:2.
13. Li YS, Ren HC, Cao JH. Correlation of SARS–CoV–2 to cancer: carcinogenic or anticancer? (review). Int J Oncol. 2022;60:42.
14. Kaufman HL, Kohlhapp FJ, Zloza A. Oncolytic viruses: a new class of immunotherapy drugs. Nat Rev Drug Discov. 2015;14:642–62.
15. Bommareddy PK, Shettigar M, Kaufman HL. Integrating oncolytic viruses in combination cancer immunotherapy. Nat Rev Immunol. 2018;18:498–513.
16. Wong RJ, Chan MK, Yu Z, Ghossein RA, Ngai I, Adusumilli PS, Stiles BM, Shah JP, Singh B, Fong Y. Angiogenesis inhibition by an oncolytic herpes virus expressing interleukin 12. Clin Cancer Res. 2004;10:4509–16.
17. Dai M, Liu D, Liu M, Zhou F, Li G, Chen Z, Zhang Z, You H, Wu M, Zheng Q, et al. Patients with Cancer Appear more vulnerable to SARS-CoV-2: a Multicenter Study during the COVID-19 outbreak. Cancer Discov. 2020;10:783–91.
18. Lee LYW, Cazier JB, Starkey T, Briggs SEW, Arnold R, Bisht V, Booth S, Campton NA, Cheng VWT, Collins G, et al. COVID-19 prevalence and mortality in patients with cancer and the effect of primary tumour subtype and patient demographics: a prospective cohort study. Lancet Oncol. 2020;21:1309–16.
19. Yang K, Sheng Y, Huang C, Jin Y, Xiong N, Jiang K, Lu H, Liu J, Yang J, Dong Y, et al. Clinical characteristics, outcomes, and risk factors for mortality in patients with cancer and COVID-19 in Hubei, China: a multicentre, retrospective, cohort study. Lancet Oncol. 2020;21:904–13.
20. He W, Chen L, Chen L, Yuan G, Fang Y, Chen W, Wu D, Liang B, Lu X, Ma Y, et al. COVID-19 in persons with haematological cancers. Leukemia. 2020;34:1637–45.
21. Bounassar-Filho JP, Boeckler-Troncoso L, Cajigas-Gonzalez J, Zavala-Cerna MG. SARS-CoV-2 as an Oncolytic Virus following reactivation of the Immune System: a review. Int J Mol Sci. 2023;24: 2326.
22. Pasin F, Mascalchi Calveri M, Calabrese A, Pizzarelli G, Bongiovanni I, Andreoli M, Cattaneo C, Rignanese G. Oncolytic effect of SARS-CoV2 in a patient with NK lymphoma. Acta Biomed. 2020;91: e2020047.
23. Challenor S, Tucker D. SARS-CoV-2-induced remission of Hodgkin lymphoma. Br J Haematol. 2021;192:415.
24. Barkhordar M, Rostami FT, Yaghmaie M, Abbaszadeh M, Chahardouli B, Mousavi SA. Spontaneous Complete Remission of Acute Myeloid Leukemia in the Absence of Disease-Modifying Therapy following Severe Pulmonary Involvement by Coronavirus Infectious Disease-19. Case Rep Hematol. 2022;2022:2603607.
25. Kandeel EZ, Refaat L, Abdel-Fatah R, Samra M, Bayoumi A, Abdellateif MS, Abdel-Hady H, Ali M, Khafagy M. Could COVID-19 induce remission of acute leukemia? Hematology. 2021;26:870–3.
26. Sollini M, Gelardi F, Carlo-Stella C, Chiti A. Complete remission of follicular lymphoma after SARS-CoV-2 infection: from the flare phenomenon to the abscopal effect. Eur J Nucl Med Mol Imaging. 2021;48:2652–4.
27. Ottaiano A, Scala S, D'Alterio C, Trotta A, Bello A, Rea G, Picone C, Santorsola M, Petrillo A, Nasti G. Unexpected tumor reduction in metastatic colorectal cancer patients during SARS-Cov-2 infection. Ther Adv Med Oncol. 2021;13:17588359211011455.
28. Choong OK, Jakobsson R, Bergdahl AG, Brunet S, Kärmander A, Waldenström J, Arvidsson Y, Altiparmak G, Nilsson JA, Karlsson J. SARS-CoV-2 replicates and displays oncolytic properties in clear cell and papillary renal cell carcinoma. PLoS ONE. 2023;18:e0279578.
29. Zhu N, Zhang D, Wang W, Li X, Yang B, Song J, Zhao X, Huang B, Shi W, Lu R, et al. A novel coronavirus from patients with Pneumonia in China, 2019. N Engl J Med. 2020;382:727–33.
30. Lamers MM, Beumer J, van der Vaart J, Knoops K, Puschhof J, Breugem TI, Ravelli RBG, Paul van Schayck J, Mykytyn AZ, Duimel HQ, et al. SARS-CoV-2 productively infects human gut enterocytes. Science. 2020;369:50–4.

31. Pan L, Mu M, Yang P, Sun Y, Wang R, Yan J, Li P, Hu B, Wang J, Hu C, et al. Clinical characteristics of COVID-19 patients with Digestive symptoms in Hubei, China: a Descriptive, cross-sectional, Multicenter Study. Am J Gastroenterol. 2020;115:766–73.
32. Jansen J, Reimer KC, Nagai JS, Varghese FS, Overheul GJ, de Beer M, Roverts R, Daviran D, Fermin LAS, Willemsen B, et al. SARS-CoV-2 infects the human kidney and drives fibrosis in kidney organoids. Cell Stem Cell. 2022;29:217–e231218.
33. Hu LL, Wang WJ, Zhu QJ, Yang L. [Novel coronavirus pneumonia-related liver injury: etiological analysis and treatment strategy]. Zhonghua Gan Zang Bing Za Zhi. 2020;28:97–9.
34. Zhang C, Shi L, Wang FS. Liver injury in COVID-19: management and challenges. Lancet Gastroenterol Hepatol. 2020;5:428–30.
35. Han Y, Duan X, Yang L, Nilsson-Payant BE, Wang P, Duan F, Tang X, Yaron TM, Zhang T, Uhl S, et al. Identification of SARS-CoV-2 inhibitors using lung and colonic organoids. Nature. 2021;589:270–5.
36. Zhou J, Li C, Liu X, Chiu MC, Zhao X, Wang D, Wei Y, Lee A, Zhang AJ, Chu H, et al. Infection of bat and human intestinal organoids by SARS-CoV-2. Nat Med. 2020;26:1077–83.
37. Bojkova D, Klann K, Koch B, Widera M, Krause D, Ciesek S, Cinatl J, Münch C. Proteomics of SARS-CoV-2-infected host cells reveals therapy targets. Nature. 2020;583:469–72.
38. Ju X, Zhu Y, Wang Y, Li J, Zhang J, Gong M, Ren W, Li S, Zhong J, Zhang L, et al. A novel cell culture system modeling the SARS-CoV-2 life cycle. PLoS Pathog. 2021;17:e1009439.
39. Perdikari TM, Murthy AC, Ryan VH, Watters S, Naik MT, Fawzi NL. SARS-CoV-2 nucleocapsid protein phase-separates with RNA and with human hnRNPs. EMBO J. 2020;39:e106478.
40. Gupta A, Madhavan MV, Sehgal K, Nair N, Mahajan S, Sehrawat TS, Bikdeli B, Ahluwalia N, Ausiello JC, Wan EY, et al. Extrapulmonary manifestations of COVID-19. Nat Med. 2020;26:1017–32.
41. Guo M, Tao W, Flavell RA, Zhu S. Potential intestinal infection and faecal-oral transmission of SARS-CoV-2. Nat Rev Gastroenterol Hepatol. 2021;18:269–83.
42. Dang M, Song J. CTD of SARS-CoV-2 N protein is a cryptic domain for binding ATP and nucleic acid that interplay in modulating phase separation. Protein Sci. 2022;31:345–56.
43. Mateju D, Eichenberger B, Voigt F, Eglinger J, Roth G, Chao JA. Single-molecule imaging reveals translation of mRNAs localized to stress granules. Cell. 2020;183:1801–e18121813.
44. Wu L, Huang S, Tian W, Liu P, Xie Y, Qiu Y, Li X, Tang Y, Zheng S, Sun Y, et al. PIWI-interacting RNA-YBX1 inhibits proliferation and metastasis by the MAPK signaling pathway via YBX1 in triple-negative breast cancer. Cell Death Discov. 2024;10:7.
45. Yang WH, Bloch DB. Probing the mRNA processing body using protein macroarrays and autoantigenomics. RNA. 2007;13:704–12.
46. Cai T, Yu Z, Wang Z, Liang C, Richard S. Arginine methylation of SARS-Cov-2 nucleocapsid protein regulates RNA binding, its ability to suppress stress granule formation, and viral replication. J Biol Chem. 2021;297:100821.
47. Zheng Y, Deng J, Han L, Zhuang MW, Xu Y, Zhang J, Nan ML, Xiao Y, Zhan P, Liu X, et al. SARS-CoV-2 NSP5 and N protein counteract the RIG-I signaling pathway by suppressing the formation of stress granules. Signal Transduct Target Ther. 2022;7:22.
48. Liu H, Bai Y, Zhang X, Gao T, Liu Y, Li E, Wang X, Cao Z, Zhu L, Dong Q, et al. SARS-CoV-2 N protein antagonizes stress Granule Assembly and IFN production by interacting with G3BPs to facilitate viral replication. J Virol. 2022;96:e0041222.
49. Chen S, Zhang J, Zhao F. Screening Linear and circular RNA transcripts from stress granules. Genomics Proteom Bioinf. 2023;21:886–93.
50. Chenon MT, Werbelow LG. An NMR study of the solution dynamics of deltorphin-I. J Am Chem Soc. 2002;124:14066–74.
51. Gao J, Zhao Y, Li T, Gan X, Yu H. The Role of PKM2 in the Regulation of Mitochondrial Function: Focus on Mitochondrial Metabolism, Oxidative Stress, Dynamic, and Apoptosis. PKM2 in Mitochondrial Function. Oxid Med Cell Longev. 2022;2022:7702681.
52. Liang J, Cao R, Wang X, Zhang Y, Wang P, Gao H, Li C, Yang F, Zeng R, Wei P, et al. Mitochondrial PKM2 regulates oxidative stress-induced apoptosis by stabilizing Bcl2. Cell Res. 2017;27:329–51.
53. Steiner S, Kratzel A, Barut GT, Lang RM, Aguiar Moreira E, Thomann L, Kelly JN, Thiel V. SARS-CoV-2 biology and host interactions. Nat Rev Microbiol. 2024;22:206–25.
54. Marcelo A, Koppenol R, Almeida LP, Matos CA, Nóbrega C. Stress granules, RNA-binding proteins and polyglutamine diseases: too much aggregation? Cell Death Dis. 2021;12:592.
55. Li T, Zeng Z, Fan C, Xiong W. Role of stress granules in tumorigenesis and cancer therapy. Biochim Biophys Acta Rev Cancer. 2023;1878:189006.
56. Mordovkina D, Lyabin DN, Smolin EA, Sogorina EM, Ovchinnikov LP, Eliseeva I. Y-Box binding proteins in mRNP Assembly, translation, and Stability Control. Biomolecules. 2020;10: 591.
57. Tian W, Zhu L, Luo Y, Tang Y, Tan Q, Zou Y, Chen K, Deng X, Tang H, Li H, et al. Autophagy Deficiency Induced by SAT1 Potentiates Tumor Progression in Triple-negative breast Cancer. Adv Sci (Weinh). 2024;11:e2309903.
58. Yuan Z, Li B, Liao W, Kang D, Deng X, Tang H, Xie J, Hu D, Chen A. Comprehensive pan-cancer analysis of YBX family reveals YBX2 as a potential biomarker in liver cancer. Front Immunol. 2024;15:1382520.
59. Tennant DA, Durán RV, Gottlieb E. Targeting metabolic transformation for cancer therapy. Nat Rev Cancer. 2010;10:267–77.
60. Alquraishi M, Puckett DL, Alani DS, Humidat AS, Frankel VD, Donohoe DR, Whelan J, Bettaieb A. Pyruvate kinase M2: a simple molecule with complex functions. Free Radic Biol Med. 2019;143:176–92.
61. Rabinowitz JD, Enerbäck S. Lactate: the ugly duckling of energy metabolism. Nat Metab. 2020;2:566–71.
62. Macedo N, Miller DM, Haq R, Kaufman HL. Clinical landscape of oncolytic virus research in 2020. J Immunother Cancer. 2020;8:e001486.
63. Shalhout SZ, Miller DM, Emerick KS, Kaufman HL. Therapy with oncolytic viruses: progress and challenges. Nat Rev Clin Oncol. 2023;20:160–77.
64. Kennedy EM, Denslow A, Hewett J, Kong L, De Almeida A, Bryant JD, Lee JS, Jacques J, Feau S, Hayes M, et al. Development of intravenously administered synthetic RNA virus immunotherapy for the treatment of cancer. Nat Commun. 2022;13:5907.

Publisher's note